Atacama Cosmology Telescope: Constraints on cosmic birefringence

Toshiya Namikawa,[1,][*] Yilun Guan,[2] Omar Darwish,[1] Blake D. Sherwin,[1] Simone Aiola,[3] Nicholas Battaglia,[4] James A. Beall,[5] Daniel T. Becker,[5] J. Richard Bond,[6] Erminia Calabrese,[7] Grace E. Chesmore,[8] Steve K. Choi,[4] Mark J. Devlin,[9] Joanna Dunkley,[10,11] Rolando Dünner,[12] Anna E. Fox,[5] Patricio A. Gallardo,[13] Vera Gluscevic,[14] Dongwon Han,[15,3] Matthew Hasselfield,[3] Gene C. Hilton,[5] Adam D. Hincks,[6] Renée Hložek,[16,17] Johannes Hubmayr,[18] Kevin Huffenberger,[19] John P. Hughes,[20] Brian J. Koopman,[21] Arthur Kosowsky,[2] Thibaut Louis,[22] Marius Lungu,[11] Amanda MacInnis,[15] Mathew S. Madhavacheril,[23,10] Maya Mallaby-Kay,[8] Loïc Maurin,[24] Jeffrey McMahon,[25,26,27,28] Kavilan Moodley,[29] Sigurd Naess,[3] Federico Nati,[30] Laura B. Newburgh,[31] John P. Nibarger,[5] Michael D. Niemack,[32,4] Lyman A. Page,[11] Frank J. Qu,[1] Naomi Robertson,[33] Alessandro Schillaci,[34] Neelima Sehgal,[15,3] Cristóbal Sifón,[35] Sara M. Simon,[36] David N. Spergel,[10,3] Suzanne T. Staggs,[11] Emilie R. Storer,[11] Alexander van Engelen,[37] Jeff van Lanen,[5] and Edward J. Wollack[38]

[1]*Department of Applied Mathematics and Theoretical Physics, University of Cambridge, Wilberforce Road, Cambridge CB3 0WA, United Kingdom*
[2]*Department of Physics and Astronomy, University of Pittsburgh, Pittsburgh, Pennsylvania 15260, USA*
[3]*Center for Computational Astrophysics, Flatiron Institute, 162 5th Avenue, New York, New York 10010, USA*
[4]*Department of Astronomy, Cornell University, Ithaca, New York 14853, USA*
[5]*National Institute of Standards and Technology, 325 Broadway, Boulder, Colorado 80305, USA*
[6]*Canadian Institute for Theoretical Astrophysics, University of Toronto, 60 St. George Street, Toronto, Ontario M5S 3H8, Canada*
[7]*School of Physics and Astronomy, Cardiff University, Cardiff CF10 3AT, United Kingdom*
[8]*Department of Physics, University of Michigan, Ann Arbor, Michigan 48109, USA*
[9]*Department of Physics and Astronomy, University of Pennsylvania, 209 South 33rd Street, Philadelphia, Pennsylvania 19104, USA*
[10]*Department of Astrophysical Sciences, Princeton University, 4 Ivy Lane, Princeton, New Jersey 08544, USA*
[11]*Joseph Henry Laboratories of Physics, Jadwin Hall, Princeton University, Princeton, New Jersey 08544, USA*
[12]*Instituto de Astrofísica and Centro de Astro-Ingeniería, Facultad de Física, Pontificia Universidad Católica de Chile, Avenida Vicuña Mackenna 4860, 7820436, Macul, Santiago, Chile*
[13]*Department of Physics, Cornell University, Ithaca, New York 14853, USA*
[14]*Department of Physics and Astronomy, University of Southern California, Los Angeles, California 90089-0484, USA*
[15]*Physics and Astronomy Department, Stony Brook University, Stony Brook, New York 11794, USA*
[16]*Dunlap Institute for Astronomy and Astrophysics, University of Toronto, 50 St. George Street, Toronto, Ontario M5S 3H4, Canada*
[17]*David A. Dunlap Department of Astronomy and Astrophysics, University of Toronto, 50 St. George Street, Toronto, Ontario M5S 3H4, Canada*
[18]*Quantum Sensors Group, NIST, Boulder, 325 Broadway, Boulder, Colorado 80305, USA*
[19]*Department of Physics, Florida State University, 609 Keen Physics Building, Tallahassee, Florida 32306, USA*
[20]*Department of Physics and Astronomy, Rutgers University, 136 Frelinghuysen Road, Piscataway, New Jersey 08854-8019, USA*
[21]*Department of Physics, Yale University, New Haven, Connecticut 06511, USA*
[22]*Universit Paris-Saclay, CNRS/IN2P3, IJCLab, 91405 Orsay, France*
[23]*Centre for the Universe, Perimeter Institute for Theoreticaxl Physics, Waterloo, Ontario N2L 2Y5, Canada*
[24]*Université Paris-Saclay, CNRS, Institut d'astrophysique spatiale, 91405 Orsay, France*
[25]*Kavli Institute for Cosmological Physics, University of Chicago, 5640 South Ellis Avenue, Chicago, Illinois 60637, USA*
[26]*Department of Astronomy and Astrophysics, University of Chicago, 5640 South Ellis Avenue, Chicago, Illinois 60637, USA*
[27]*Department of Physics, University of Chicago, Chicago, Illinois 60637, USA*
[28]*Enrico Fermi Institute, University of Chicago, Chicago, Illinois 60637, USA*
[29]*Astrophysics and Cosmology Research Unit, School of Mathematics, Statistics & Computer Science, University of KwaZulu-Natal, Durban 4041, South Africa*

[30]*Department of Physics, University of Milano - Bicocca,*
Piazza della Scienza, 3 - 20126, Milano (MI), Italy
[31]*Department of Physics, Yale University, New Haven, Connecticut 06520, USA*
[32]*Department of Physics, Cornell University, 109 Clark Hall, Ithaca, New York 14853, USA*
[33]*Institute of Astronomy, University of Cambridge,*
Madingley Road, Cambridge CB3 0HA, United Kingdom
[34]*Department of Physics, California Institute of Technology, Pasadena, California 91125, USA*
[35]*Instituto de Física, Pontificia Universidad Católica de Valparaíso, Casilla 4059, Valparaíso, Chile*
[36]*Department of Physics, University of Michigan, 450 Church Street, Ann Arbor, Michigan 48109, USA*
[37]*School of Earth and Space Exploration, Arizona State University, Tempe, Arizona 85287, USA*
[38]*NASA Goddard Spaceflight Center, 8800 Greenbelt Road, Greenbelt, Maryland 20771, USA*

We present new constraints on anisotropic birefringence of the cosmic microwave background polarization using two seasons of data from the Atacama Cosmology Telescope covering 456 square degrees of sky. The birefringence power spectrum, measured using a curved-sky quadratic estimator, is consistent with zero. Our results provide the tightest current constraint on birefringence over a range of angular scales between 5 arc minutes and 9°. We improve previous upper limits on the amplitude of a scale-invariant birefringence power spectrum by a factor of between 2 and 3. Assuming a nearly massless axion field during inflation, our result is equivalent to a 2σ upper limit on the Chern-Simons coupling constant between axions and photons of $g_{\alpha\gamma} < 4.0 \times 10^{-2}/H_I$, where H_I is the inflationary Hubble scale.

I. INTRODUCTION

The Atacama Cosmology Telescope (ACT) experiment, a 6-m-diameter millimeter-band telescope located in the Atacama Desert in Chile, has completed several seasons of cosmic microwave background (CMB) polarization observations [1]. These observations have been used to derive a variety of scientific results—for example, via measurements of the CMB power spectrum [2] and gravitational lensing by large-scale structure [3,4]. Beyond these observables, ACT's CMB polarization data can be used to test for new physics by searching for a rotation of linear polarization as the CMB photons propagate to us from the surface of last scattering. This phenomenon, which is absent in the Standard Model, is referred to as cosmic birefringence.

Several types of beyond-the-Standard-Model physics can source cosmic birefringence. In particular, birefringence of CMB photons can be generated by axionlike particles within a mass range of $10^{-33} \lesssim m_a \lesssim 10^{-28}$ eV that couple to photons through a so-called Chern-Simons term (see, e.g., Refs. [5–9] and a review, Ref. [10]).[1] The existence of such axionlike particles is a generic prediction of string theory. In addition, birefringence-inducing pseudoscalar fields could be candidates for an early dark energy

mechanism to resolve the current Hubble parameter tension [12]. Cosmic birefringence can be used as a probe of, e.g., the axion string network [13], axion dark matter [14], and also more general Lorentz-violating physics in the context of Standard Model extensions [15]. Finally, cosmic birefringence can also be generated by primordial magnetic fields (PMFs) through Faraday rotation of the CMB polarization (e.g., Refs. [16–21]). The PMF-induced cosmic birefringence has frequency dependence and can be distinguished from that induced by axionlike particles [22]. If the source of the cosmic birefringence is spatially varying, the polarization rotation will be anisotropic (i.e., have different values in different directions in the sky); indeed, anisotropies in the cosmic birefringence are produced naturally by many of the types of beyond-the-Standard-Model physics listed previously (see, e.g., Refs. [5,15,23–26]). For example, quintessence models predict both isotropic and anisotropic cosmic birefringence [25]. In addition, the cosmic birefringence induced by some massless scalar fields does not necessarily produce isotropic cosmic birefringence, and a measurement of the anisotropic birefringence is crucial to constraining such scenarios [27]. Measurements of, or tight constraints on, the relevant pseudoscalar fields and other phenomena can hence provide valuable insights into fundamental physics.

Both isotropic and anisotropic cosmic birefringence have been constrained by several CMB experiments, although the observational effects on the CMB and the methodology to measure these two types of birefringence are different. The presence of isotropic cosmic birefringence can be detected in CMB observations because the polarization

---

*Corresponding author.
tn334@cam.ac.uk
[1]Axionlike particles within a mass range of $10^{-22} \lesssim m_a \lesssim 10^{-18}$ eV also introduce a time variation of the polarization angle rotation whose oscillation period is from hours to years, and can be tightly constrained by current and future CMB experiments, as discussed in Ref. [11].

rotation transfers part of the CMB E-mode polarization to B modes and thus creates nonzero odd-parity EB power spectra. Such odd-parity EB power spectra are zero in the standard cosmological model and have hence been used for constraining isotropic cosmic birefringence [28–31]. However, odd-parity power spectra have systematic uncertainties from the global polarization angle calibration [32–36]; in fact, odd-parity spectra are often used to calibrate the global polarization angle rather than for measuring cosmological signals [37,38]. Galactic foreground components in the observed odd-parity spectra can be used to partially break degeneracies between the global polarization angle error and cosmic birefringence effects [39], although the signal-to-noise ratio can decrease somewhat in this process.

On the other hand, if the cosmic birefringence is anisotropic, we can measure it not only using CMB power spectra [7] but also by using the fact that the EB correlation varies with direction, which is characteristic of statistical anisotropy [40]. Variations of the polarization rotation angle on angular scale L will mix together E and B modes of different scales, leading to nonzero expectation values in the off-diagonal ($\ell \neq \ell'$) elements of the CMB covariance [see Eq. (5) below].[2] We can, therefore, reconstruct the anisotropies of the cosmic birefringence by measuring these off-diagonal correlations, in a manner similar to CMB lensing reconstruction [41]. Other pairs of CMB anisotropies such as temperature and B modes are also correlated, but such correlations generally give lower signal-to-noise ratios for reconstructing birefringence [42]. We will therefore focus on birefringence reconstruction from EB correlations in this paper. Note that the cosmic birefringence and lensing can be estimated separately by using their distinct effects on polarization maps in terms of parity [40]; birefringence introduces rotations with determinate directions, and the resulting map is not parity symmetric, whereas lensing arising from the scalar density field has even parity (see Sec. III for details).

Multiple publications have presented constraints on anisotropies of the cosmic birefringence using reconstruction methods; these have made use of the WMAP temperature and B modes [27], or the polarization data of the POLARBEAR [43], BICEP2/Keck Array [44], and Planck [45] experiments. The use of the reconstructed cosmic birefringence power spectrum is the most powerful current method for measuring the anisotropies of the cosmic birefringence and indeed gives the best current constraints [44,45]. However, we note that several other publications [14,30,31,46–49] also place constraints on anisotropic birefringence by analyzing CMB polarization power spectra.

In this paper, we reconstruct the cosmic birefringence (rotation) field from the CMB polarization using a quadratic estimator analogous to those commonly used in measuring the cosmic deflection field due to gravitational lensing. The estimator includes the effect of sky curvature, which will become increasingly important as low-noise and high-resolution polarization maps extend over larger sky regions. We focus on frequency-independent cosmic birefringence and apply this estimator to data from the Atacama Cosmology Telescope Polarimeter (ACTPol), finding a rotation field consistent with zero within measurement uncertainties. Our limits on polarization rotation are the strongest to date over a wide range of scales.

In Sec. II, we describe our data and simulations for the cosmic birefringence reconstruction. In Sec. III, we explain our reconstruction methodology, and in Sec. IV we explore potential systematic errors that are relevant for the cosmic birefringence analysis. Section V shows our results for the reconstructed spectrum and the resulting constraint on the scale-invariant birefringence spectrum. We discuss implications for axionlike particles in Sec. VI.

II. DATA AND SIMULATIONS

We analyze ACTPol nighttime polarization data collected from two seasons of observations taken in 2014 and 2015. These data are described in Ref. [2]. In this paper, the constraints on cosmic birefringence anisotropies are derived using data from one region of the sky, which we label D56. D56 spans 456 deg^2 of the sky with the aspect ratio of 1∶4 observed in both the 2014 and 2015 seasons at 150 GHz, and in the 2015 season at 90 GHz [2,50,51]; the map has an effective noise level of 14 μK-arcmin for polarization. In addition to D56, we also use another region of the sky for a (swap-patch) null test: the region is called BOSS-N; this field was observed during the 2015 season and covers 1633 deg^2 of the sky with an effective noise level of roughly 30 μK-arcmin in polarization. Since the statistical error of the reconstructed cosmic birefringence spectrum from the BOSS-N region is roughly 4–5 times larger than that from D56, the improvement of the cosmic birefringence constraint by adding BOSS-N is roughly ≲3%.[3] Thus, we use the BOSS-N data only for a null test. For each region (D56 and BOSS-N), the Fourier-space combined E and B maps are produced from

---

[2]In this paper, we use L to denote the multipole of the reconstructed rotation angle and ℓ to denote the multipole of CMB anisotropies.

[3]The noise spectrum of the reconstructed cosmic birefringence fields scales as the fourth power of the CMB map noise if the CMB maps are noise dominant. In BOSS-N, even the EE spectrum is not signal dominant, and the reconstructed noise spectrum is roughly an order of magnitude larger than that of D56. Taking into account the sky coverage, the statistical error of the reconstructed spectrum is 4–5 times larger than that of D56. The expected improvement on the signal-to-noise ratio of the birefringence spectrum is thus negligible, $\sqrt{1 + (1/4)^2} \sim 3\%$.

the maps in each frequency, each detector array, and season [52].

We use Monte Carlo simulations for the standard ΛCDM cosmology[4] to test our pipeline, compute the biases in the power spectrum measurement, perform null tests, and calculate the covariance matrix for the χ^2 PTE and likelihood. The simulation includes lensing and realistic effects to mimic the data such as beams and inhomogeneous noise (see Refs. [2,51] for the details). Hereafter, we call this simulation the standard simulation. Additional simulations including scale-invariant rotation anisotropies with varying amplitudes A_{CB} (see Sec. V for the definition) are used for pipeline tests and to compute the transfer function for the reconstructed spectrum. To assess the impact of the global polarization angle error on our measurements, we also generate a simulation with an offset in the global polarization angle (see Sec. IV). We obtain a candidate dust map by appropriately scaling the Galactic dust simulation of Ref. [54], which provides a non-Gaussian full-sky dust Q/U map at 353 GHz.

III. ANALYSIS

The rotation angle field, $\alpha(\hat{n})$, can be reconstructed from the off-diagonal mode-mode covariance within and between the E and B modes [40]. An estimator of $\alpha(\hat{n})$ has a quadratic form similar to the lensing estimator. The power spectrum of the anisotropic rotation angle $C_L^{\alpha\alpha}$ can be obtained by squaring the rotation estimator and subtracting relevant biases. We use the curved-sky quadratic estimator to extract the large-scale birefringence anisotropies which are important to constrain the scale-invariant spectrum described later. Verification of the method to measure the cosmic birefringence spectrum applied in this paper is described in Ref. [55] for a flat-sky analysis. In the extension described here, the estimator in a full-sky formalism employs spherical harmonic transformations instead of Fourier transforms.[5]

In order to account for ground and atmospheric noise, we begin by filtering out the Fourier modes $|\ell_x| < 90$ and $|\ell_y| < 50$ of the E and B maps produced by combining seasons, frequencies, and arrays in Fourier space [52]. This is the same filter as is applied for the CMB power spectrum and lensing reconstruction analysis [2,3]. This process is performed using a flat-sky Fourier transform. After transforming back to position space, we assign the filtered E and B maps to the Healpix grids and compute the harmonic coefficients of the E and B modes. Note that the polarization maps are provided at each patch, which take into account the curved-sky geometry. The harmonic

coefficients computed from these maps thus do not have any distortion due to ignoring the curved-sky geometry. In fact, if such distortion is significant, we need additional filtering processes in computing $\bar{X}_{\ell m}$, or additional correction to the estimator normalization. As we discus below, however, we found that the mismatch between the input birefringence spectrum and cross spectrum between input and reconstructed birefringence fields is very small, and the above distortion is negligible.

The presence of the cosmic birefringence effect rotates the primordial Stokes parameters as [27,40]

$$Q'(\hat{n}) \pm iU'(\hat{n}) = [Q(\hat{n}) \pm iU(\hat{n})]e^{\pm 2i\alpha(\hat{n})}. \quad (1)$$

Consequently, the rotation angle modifies the CMB E and B modes. The E and B modes are obtained by transforming Q and U maps with the spin-2 spherical harmonics, $Y_{\ell m}^{\pm 2}$, as [56,57]

$$E_{\ell m} \pm iB_{\ell m} = -\int d^2\hat{n}(Y_{\ell m}^{\pm 2})^*[Q(\hat{n}) \pm iU(\hat{n})]. \quad (2)$$

Thus, the E and B modes in the presence of an anisotropic rotation angle are derived by substituting Eq. (1) into the above equation, and are given up to linear order in α by [40,58]

$$E'_{\ell m} \pm iB'_{\ell m}$$
$$= E_{\ell m} \pm iB_{\ell m} + \sum_{LM\ell'm'} (-1)^m \begin{pmatrix} \ell & L & \ell' \\ -m & M & m' \end{pmatrix} W_{\ell L\ell'}^{\pm}$$
$$\times [E_{\ell'm'} \pm iB_{\ell'm'}]\alpha_{LM}, \quad (3)$$

with

$$W_{\ell_1\ell_2\ell_3}^{\pm} = \pm 2\zeta^{\mp} p_{\ell_1\ell_2\ell_3}^{\mp} \sqrt{\frac{(2\ell_1+1)(2\ell_2+1)(2\ell_3+1)}{4\pi}}$$
$$\times \begin{pmatrix} \ell_1 & \ell_2 & \ell_3 \\ -2 & 0 & 2 \end{pmatrix}. \quad (4)$$

Here, $\zeta^+ = 1$, $\zeta^- = i$, and $p_{\ell_1\ell_2\ell_3}^{\pm} = [1 \pm (-1)^{\ell_1+\ell_2+\ell_3}]/2$ is a parity indicator. The ending parentheses denote the Wigner $3j$ symbol. The off-diagonal elements of the covariance induced by the anisotropies of the rotation angle are given by [58]

$$\langle E'_{\ell m} B'_{\ell'm'} \rangle_{CMB} = \sum_{LM} \begin{pmatrix} \ell & \ell' & L \\ m & m' & M \end{pmatrix} f_{\ell L\ell'}^{\alpha} \alpha_{LM}^*, \quad (5)$$

where $\ell \neq \ell'$, $m \neq -m'$, and the operator $\langle \cdots \rangle_{CMB}$ denotes an ensemble average over the realizations of CMB and noise with a fixed realization of $\alpha(\hat{n})$. The weight function is

$$f_{\ell L\ell'}^{\alpha} = -W_{\ell' L\ell}^{-} \tilde{C}_{\ell}^{EE}, \quad (6)$$

---

[4]The standard cosmology in this paper is the flat ΛCDM model parametrized by the six cosmological parameters with values close to the best-fit 2015 Planck parameters [53].

[5]The code used for reconstructing the cosmic birefringence in full sky is based on https://toshiyan.github.io/clpdoc/html/.

where $\tilde{C}_\ell^{\rm EE}$ is the lensed E-mode power spectrum. The term originating from the lensing B mode is ignored, since the improvement of the sensitivity to the polarization rotation anisotropies by the inclusion of this term is negligible [43]. Similar to the lensing reconstruction, the unnormalized quadratic estimator of α is constructed as a convolution of the E and B modes with the weight function of Eq. (6) [58]:

$$\bar{\alpha}_{LM}^* = \sum_{\ell\ell'mm'} \begin{pmatrix} \ell & \ell' & L \\ m & m' & M \end{pmatrix} f_{\ell L \ell'}^\alpha \bar{E}_{\ell m} \bar{B}_{\ell'm'}. \quad (7)$$

Here, $\bar{E}_{\ell m}$ and $\bar{B}_{\ell m}$ are the observed multipoles filtered by their inverse variance. We use diagonal filtering, $\bar{X}_{\ell m} = \hat{X}_{\ell m}/\hat{C}_\ell^{\rm XX}$, where X is either E or B and $\hat{C}_\ell^{\rm XX}$ is the power spectrum of the observed multipoles, $\hat{X}_{\ell m}$. The CMB multipoles at $200 \le \ell \le 2048$ are used for our baseline reconstruction, although we also perform the reconstruction for other multipole ranges as a test of the analysis in Sec. IV. Finally, we correct for the mean-field bias, $\langle \bar{\alpha}_{LM} \rangle$, and normalize to obtain the rotation angle:

$$\hat{\alpha}_{LM} = A_L(\bar{\alpha}_{LM} - \langle \bar{\alpha}_{LM} \rangle). \quad (8)$$

The normalization A_L is given by

$$A_L = \frac{1}{2L+1} \sum_{\ell\ell'} \frac{(f_{\ell L \ell'}^\alpha)^2}{\hat{C}_\ell^{\rm EE} \hat{C}_{\ell'}^{\rm BB}}. \quad (9)$$

We compute Eqs. (7) and (9) with a computationally efficient method, as described in Appendix A. The mean-field bias could be nonzero due to, for example, survey boundary and beam asymmetry effects [59] (see also Appendix B). We evaluate the mean-field bias by averaging over the standard simulations, finding that the bias is less than 0.5% of the 1σ statistical error of the cosmic birefringence spectrum over the scales relevant to our analysis. Mean-field bias is also induced by the global polarization angle error, which is not included in the standard simulations. We evaluate this effect in Sec. IV and discuss its origin in Appendix B.

We note that the quadratic estimator for the cosmic birefringence anisotropies given above is the same as that for the CMB lensing potential, ϕ, but with a different weight function. In the case of CMB lensing, the off-diagonal covariance of Eq. (5) is given by [41]

$$\langle \tilde{E}_{\ell m} \tilde{B}_{\ell'm'} \rangle_{\rm CMB} = \sum_{LM} \begin{pmatrix} \ell & \ell' & L \\ m & m' & M \end{pmatrix} f_{\ell L \ell'}^\phi \phi_{LM}^*, \quad (10)$$

where $\tilde{E}$ and $\tilde{B}$ are the lensed E and B modes, respectively, and f^ϕ is defined as [41]

$$f_{\ell L \ell'}^\phi = -i p_{\ell L \ell'}^- \sqrt{\frac{(2\ell+1)(2L+1)(2\ell'+1)}{16\pi}}$$
$$\times [L(L+1) + \ell(\ell+1) - \ell'(\ell'+1)]$$
$$\times \begin{pmatrix} \ell' & L & \ell \\ 2 & 0 & -2 \end{pmatrix} \tilde{C}_\ell^{\rm EE}. \quad (11)$$

Here, $p_{\ell+L+\ell'}^- = [1 - (-1)^{\ell+L+\ell'}]/2$ is the parity indicator. The estimator for the CMB lensing potential is then obtained in the same form as Eq. (7), but replacing f with f^ϕ. The normalization is also obtained in the same way. The main difference between the properties of f^α and f^ϕ is that f^α and f^ϕ are only nonzero when $\ell + L + \ell'$ is even for f^α and odd for f^ϕ [40]. This property comes from the difference of the parity symmetry between the lensing potential and cosmic birefringence anisotropies. With this property of f^α and f^ϕ, our standard estimators can completely separate the cosmic birefringence and lensing potential contributions to the off-diagonal elements of the EB correlation, similar to the lensing potential and curl mode decomposition [60].

From the reconstructed α, the cosmic birefringence spectrum is also estimated in the same way as the CMB lensing power spectrum [3,61], but with a few modifications. The power spectrum of the estimator defined in Eq. (8) is a four-point function and has a disconnected (or Gaussian) bias, N_L^0, which is simply due to the original, unrotated CMB anisotropies and is nonzero even in the absence of birefringence [41,55,62]. We construct an estimator of the disconnected bias, $\widehat{N_L^0}$, using a realization-dependent algorithm [59], and subtract it from the power spectrum of the estimator to extract the cosmic birefringence spectrum. For simulations, for convenience we subtract the ensemble average, $\langle \widehat{N_L^0} \rangle$, instead of $\widehat{N_L^0}$, which makes less than 1% difference in the χ^2 PTE of the reconstructed cosmic birefringence spectrum and the constraints on the scale-invariant spectrum. Using a realization-dependent bias subtraction makes our measurement of the birefringence spectrum robust to possible mismatches between simulation and data. The lensing bias and N1 bias as shown in Ref. [55] are evaluated using simulation from the standard and nonzero birefringence simulations, respectively. The lensing bias is subtracted from the reconstructed birefringence spectrum, and the N1 bias is included in modeling the signal spectrum of the cosmic birefringence. They are, however, negligible compared to the 1σ statistical error of the reconstructed birefringence spectrum.

Using a simulation with nonzero birefringence, we confirm that the cross spectrum between the input and reconstructed birefringence anisotropies agrees with the input spectrum to within 0.3% for multipoles $L \ge 20$, and so we do not apply a transfer function to correct the normalization of the reconstructed spectrum.

In this paper, we compute the cosmic birefringence power spectrum up to $L \leq 2048$. At larger L values, the statistical uncertainties of the reconstructed spectrum start to increase significantly. The minimum multipole of the reconstructed spectrum is chosen so that the mean-field bias from the global polarization angle uncertainties is negligible (see Sec. IV).

IV. POTENTIAL SYSTEMATICS

The ACT polarization data have been tested for possible systematic errors in several published or forthcoming papers focusing on the CMB power spectrum [2], lensing 3]], and cross spectra with galaxy surveys [52]. Here, we further test for potential systematic contamination which could specifically bias the measured cosmic birefringence spectrum. Here and in the following sections, we use 200 realizations of the simulations to evaluate the band-power covariance matrix for the cosmic birefringence spectrum, as well as the chi-squared probability to exceed (PTE).

A. Uncertainties in polarization angle measurement

Global polarization angle errors induce nonzero odd-parity power spectra [34,37]. We estimate a constant global rotation angle ψ as follows: Assuming $|\psi| \ll 1$, the global rotation angle is related to the polarization spectra as $\psi = C_b^{EB}/2(C_b^{EE} - C_b^{BB}) \equiv a_b$ at each multipole bin b [34]. We compute the angle by minimizing $\sum_{bb'}(\psi - \hat{a}_b)\text{Cov}_{bb'}^{-1}(\psi - \hat{a}_{b'})$, where $\hat{a}_b$ is the observed value of a_b and Cov is the covariance of a_b computed from 200 realizations of the standard simulation. With the polarization spectra at $200 \leq \ell \leq 2048$, we find that $\psi = 0.12° \pm 0.06°$. The 1σ uncertainty of the global rotation angle introduces a significant mean-field bias at very large scales (see Appendix B for the origin of the bias). The mean-field bias only becomes close to the 1σ statistical error of the cosmic birefringence spectrum at $L \ll 20$. We therefore exclude the large-scale cosmic birefringence spectrum, $L < 20$, from our analysis. Note that this scale roughly corresponds to the fundamental mode determined by our patch size. The measured spectrum below this multipole does not have much information on cosmic birefringence signals.

An additional possible concern is the variation of polarization angle errors over the field. Variations in relative polarization angles between detectors are calibrated based on optical modeling of the telescope and instrument [63]. In order to obtain variation of polarization angle errors over the field at a significant level, one would require that (i) different detectors have significantly different polarization angle errors; (ii) the relative weights of different detectors vary strongly over the map (since otherwise differential detector angle errors would be absorbed into the mean); and (iii) such an effect not be significantly reduced by averaging from repeated scanning (which it

should be, as the main driver of the relative detector weight is the atmospheric loading and thermal environment in the telescope, not which sky direction is being observed). Another potential source of the variation of polarization angle in the field is due to our mapmaking process. In the coordinate transformation from focal plane to horizontal plane for each map obtained from each season, frequency, and array, we corrected the coordinate rotation using the angle estimated by the *EB* spectrum, instead of the exact value of the rotation angle, for computational convenience. We checked that the resulting angle corrections using this method and with the exact coordinate rotation angle agree with each other, but this process could lead to small angle errors depending on the elevation of our scan. Since all of these effects are individually unlikely to be large, the likelihood of all these taking place at a significant level is very small, and we therefore neglect such effects. (This is further motivated by the fact that potential upper limits are not degraded by any such systematic, since the systematic is not correlated with a true birefringence signal. As both birefringence and polarization angle error spectra must give strictly positive contributions to the estimated birefringence power spectrum, the presence of such a systematic would, in fact, imply stronger constraints on cosmological birefringence from a data-derived upper limit.)

B. Galactic foregrounds

The large-scale *B* modes are significantly contaminated by Galactic foregrounds, and in principle, non-Gaussian polarized foregrounds could also bias the measured birefringence spectrum. We expect minimal direct contamination from the Galactic foregrounds since our analysis removes multipoles below $\ell = 200$ from the maps before reconstructing the cosmic birefringence anisotropies. For an accurate estimate of any bias to the cosmic birefringence anisotropies, however, we further test the Galactic foreground contributions to our measurement by adding a simulation of Galactic dust to our standard simulation. In particular, we use 20 different realizations of the Galactic dust simulation provided by Ref. [54] in the D56 region for this purpose. We scale the dust polarization maps to our observing frequencies following Refs. [64,65]; we assume a modified blackbody spectrum for dust and use the dust spectral index and temperature of Ref. [65]. We then add the scaled polarization maps to 20 realizations of the input of our standard CMB simulation to produce a set of 20 simulations including dust. Figure 1 shows the difference spectrum between the simulations including dust and the standard simulations averaged over 20 realizations. The spectrum is further normalized by the 1σ statistical error of the cosmic birefringence spectrum obtained from 200 realizations of the standard simulation. Although we do not yet have sufficient multifrequency data to fully exclude any impact of Galactic foregrounds, we find that the impact of the dust contribution estimated from our simulations is
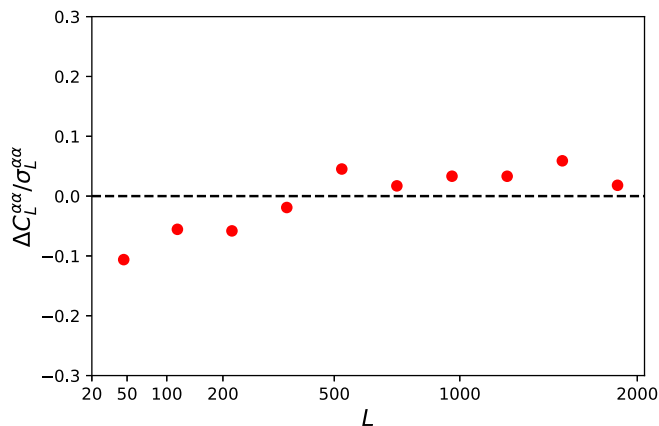
FIG. 1. The difference of the cosmic birefringence spectra between the standard plus Galactic dust and standard simulations. Each value has been divided by the 1σ statistical uncertainty in the standard cosmic birefringence spectrum.

approximately less than 10% of the 1σ statistical uncertainty at each multipole bin.

C. Null tests

As a null test, we compute the cross spectrum of the reconstructed α obtained from the D56 and BOSS-N fields. The reconstructed cosmic birefringence anisotropies on these two patches should not be correlated, and so the cross spectrum should be zero. Following the same procedures as applied to the D56 field, the harmonic coefficients of the cosmic birefringence anisotropies from BOSS-N are reconstructed using the curved-sky quadratic estimator described in Sec. III and are then cross-correlated with the birefringence map from D56. This null spectrum can serve as a valuable test of whether our error bars are correct. Figure 2 shows the cross spectrum; we find that the χ^2 PTE of the cross spectrum is within 2σ range, and the spectrum is consistent with null.
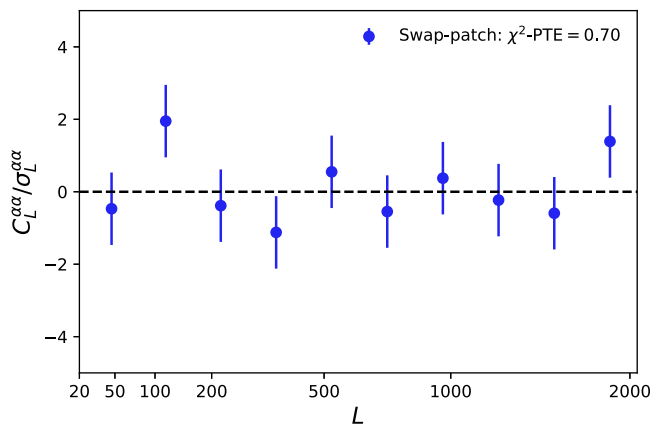
For additional null tests, we compute the difference between the baseline analysis and cases with different choices of CMB multipole ranges used for the rotation angle reconstruction. Figure 2 shows the difference spectra. We calculate the χ^2 PTE for the difference spectra as shown in the figure, finding that the difference spectra are consistent with the null hypothesis, irrespective of the choice of the CMB multipole range.

V. RECONSTRUCTED SPECTRUM

After passing the swap-patch and difference spectrum null tests in Sec. IV, we unblinded the reconstructed cosmic birefringence spectrum. Figure 3 shows the cosmic birefringence spectrum from ACTPol data with errors obtained from the standard simulation. For comparison, the figure also shows the cosmic birefringence power spectra measured from other recent CMB experiments: the BICEP2/ Keck Array [44], POLARBEAR [43], and Planck [45]. Compared to other experiments, ACTPol provides the tightest constraint on the cosmic birefringence spectrum at $20 \leq L \leq 2048$. We compute the χ^2 PTE of our measured spectrum including covariance obtained from simulation, and the value is found to be 0.99; this is in good agreement with zero signal. We note that the off-diagonal elements of the correlation matrix for this measurement become ~ 0.5 at $L > 1000$, while at lower L, off-diagonal band-power correlations are negligible.

The χ^2 PTE is close to unity; to investigate this further (and test whether this result indicates an overestimate of our error bars), we check the dependency of the χ^2 PTE on analysis choices and summarize in Table I, finding that the value is typically less than 0.95. Note that the values in Table I are not statistically independent from the baseline value, since we only modify the analyzed data by a small amount by changing $L_{\min}$ (and changing the number of multipole bins does not introduce any new data). However,
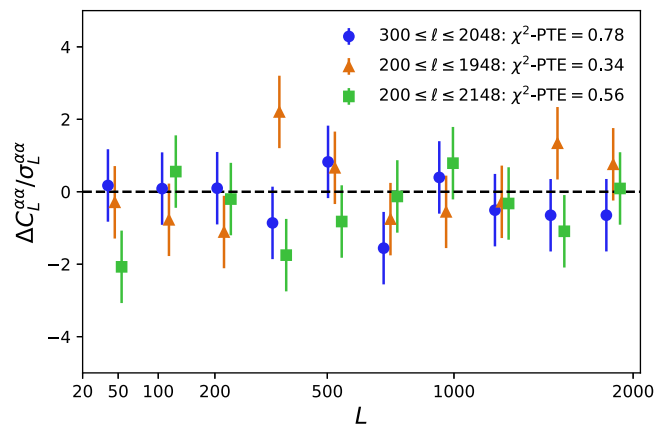

FIG. 2. The null cosmic birefringence spectra for the swap patch (*left*) and difference spectra (*right*) tests, each divided by the statistical 1σ error of the spectrum. For the swap patch, we show the cross spectrum of the reconstructed cosmic birefringence anisotropies between two separate patches of sky, D56 and BOSS-N.
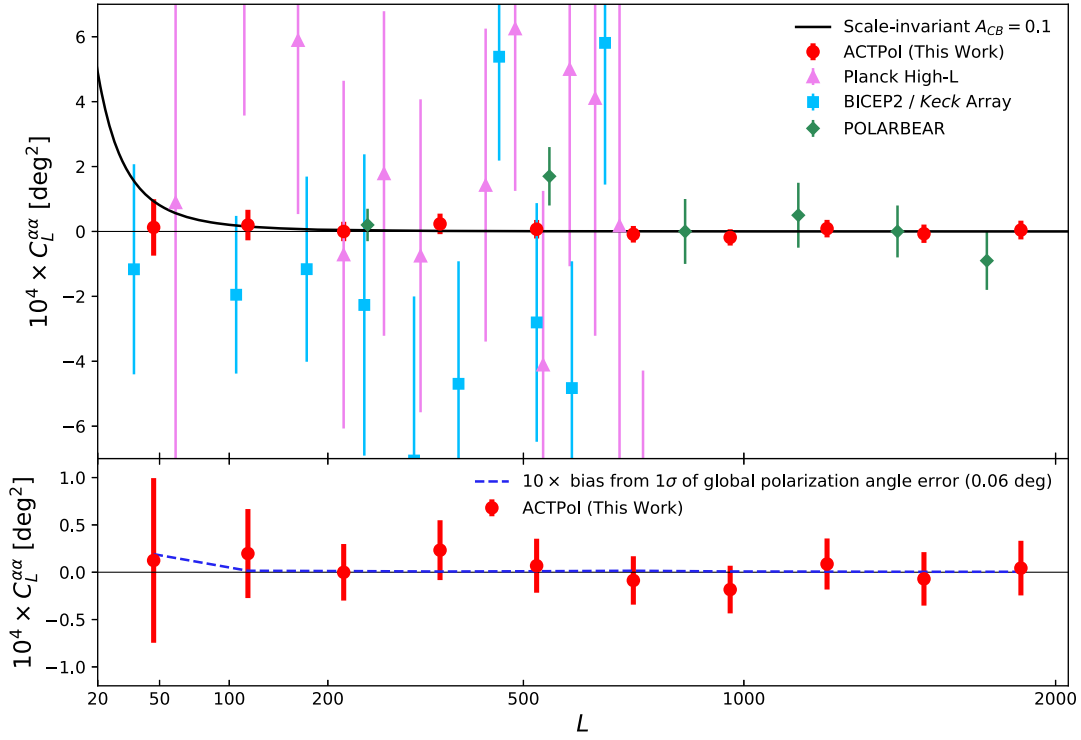
FIG. 3. The angular power spectrum of the polarization rotation fields $\alpha(\hat{n})$ measured from ACTPol data over 456 deg^2 of sky, with errors from a standard ΛCDM simulation. The solid line shows a scale-invariant spectrum with the amplitude corresponding to our 2σ upper bound (see Sec. V). In addition to our work (red), we also show the spectra obtained from POLARBEAR (green) [43], the BICEP2/Keck Array (blue) [44], and Planck (magenta) [45]. The Planck low-L results are not included due to the error bar size. The lower panel shows a zoomed-in view of our birefringence power spectrum measurement; we also show, with a blue dotted line, the potential bias from a global polarization angle systematic error of 0.06°, which is of the same size as the 1σ error from an EB-derived constraint. Since this is difficult to see, for visualization, we have multiplied this angle error bias by a factor of 10.

if we had significantly overestimated our error bars, we would expect that these other scale ranges and binnings would also have very high PTE values. In addition, as described previously, we have performed several null tests where simulations are used to evaluate the scatter, without finding anomalous PTEs. The high χ^2 PTE for the baseline spectrum therefore is likely due to a statistical fluctuation rather than an overestimate of the errors. Of course, if in fact the errors have been slightly overestimated, our limit on the cosmic birefringence will be somewhat conservative.

The minimum CMB multipole used in the cosmic birefringence reconstruction is 200, which is lower than

TABLE I. The χ^2 PTE values for our measured cosmic birefringence spectrum with variation of the minimum multipole, $L_{\min}$, or the number of multipole bins, N_b. For the baseline analysis, where $L_{\min} = 20$ and $N_b = 10$, the PTE is 0.99; the variation seen in this table, given different analysis choices, is consistent with this high PTE being a fluctuation.

$L_{\min}$	χ^2 PTE	N_b	χ^2 PTE
10	0.85	15	0.77
30	0.94	20	0.88

that of the lensing measurement presented in Ref. [3]. In that lensing analysis, the CMB multipoles below $\ell = 500$ are removed, since the simulations are not consistent with temperature data at these scales due to inaccurate atmospheric noise characterization and transfer function estimation. For this analysis, however, the temperature data are not used, and the measured polarization noise spectrum is consistent with simulations for $\ell \geq 200$. In addition, as demonstrated by our null test in Fig. 2, changing the minimum multipole used does not produce any spurious signals. To further test this, we evaluate the χ^2 PTE of a measured spectrum analyzed with $\ell_{\min} = 300$, finding that the value effectively does not change from the case with $\ell_{\min} = 200$; in addition, all our null tests still pass. These facts indicate that the inclusion of low-ℓ CMB polarization does not introduce non-negligible systematics into our measurement.

As an example of the implications of our measurement for phenomenological models of cosmic birefringence, we consider a constraint on the amplitude of the scale-invariant spectrum, $C_L^{\alpha\alpha} \propto 2\pi/L(L+1)$, which can be later translated into, for example, a constraint on the coupling constant of an axionlike particle. To constrain a scale-invariant spectrum, we first construct an approximate

likelihood for the reconstructed cosmic birefringence power spectrum. Although we do not use multipoles at $L < 20$, the distribution of the power spectrum in the largest bin is asymmetric and is not well described by a Gaussian. Instead, we assume the log-likelihood proposed by Ref. [66]:

$$-2\ln\mathcal{L}(\hat{A}) = \sum_{bb'} g(c_b^0 \hat{A}_b)[c_b^1 C_b^f]\mathrm{Cov}_{bb'}^{-1}[c_{b'}^1 C_{b'}^f]g(c_{b'}^0 \hat{A}_{b'}),$$

(12)

where $\hat{A}_b = (\hat{C}_b^{\alpha\alpha} + \langle\hat{N}_b^0\rangle)/(C_b^{\alpha\alpha} + \langle\hat{N}_b^0\rangle)$ is the amplitude of the quadratic-estimator power spectrum relative to that including the cosmic birefringence signals, $C_b^{\alpha\alpha}$, at each multipole bin, b, and $g(x) = \mathrm{sign}(x-1)\sqrt{2(x-\ln x-1)}$ for $x \geq 0$. Note that $C_b^{\alpha\alpha}$ is the sum of the scale-invariant birefringence spectrum and N1 bias evaluated from the nonzero birefringence simulation. The power spectrum, C_b^f, and covariance, $\mathrm{Cov}_{bb'}$, are evaluated by the mean and variance of the quadratic-estimator power spectrum from the standard simulation, respectively. Note that we further introduce parameters, c_b^0, c_b^1, to make the above likelihood closer to that obtained from the simulation. We compute c_b^0 and c_b^1 by fitting the histogram of $\hat{A}_b$ from the simulation using Eq. (12) at each bin. (We verified that the values of c_b^0 and c_b^1 only vary by negligible amounts using simulations containing different levels of birefringence signal.)

Using Eq. (12), we compute the likelihood for the amplitude of the scale-invariant power spectrum defined by $L(L+1)C_L^{\alpha\alpha}/2\pi = A_{\mathrm{CB}} \times 10^{-4}$ [rad^2]. Assuming a flat prior for $A_{\mathrm{CB}} \geq 0$, we then obtain the 2σ upper limit on the amplitude as $A_{\mathrm{CB}} \leq 0.10$ (which is equivalent to $L(L+1)C_L^{\alpha\alpha}/2\pi \leq 0.033$ [deg^2]). This constraint improves the previous best constraints by a factor of between 2 and 3 [44,45]. Note that, for the scale-invariant power spectrum, the constraint on its amplitude is mostly determined by the largest-scale multipole bin; removing the first multipole bin centered at $L = 47$ degrades the constraint considerably.

VI. DISCUSSION

Our measured spectrum can be used to constrain various models which lead to cosmic birefringence anisotropies. As an example, we consider the following interaction between axionlike particles and photons in the Lagrangian [67]:

$$\mathcal{L} \supset \frac{g_{a\gamma}a}{4}F_{\mu\nu}\tilde{F}^{\mu\nu},$$

(13)

where $g_{\alpha\gamma}$ is the Chern-Simons coupling constant between the axionlike particles and photon, a is the axionlike particle field, $F_{\mu\nu}$ is the electromagnetic field, and $\tilde{F}^{\mu\nu}$ is its dual. The presence of axionlike particles produces a rotation of the polarization angle as [67,68]

$$\alpha = \frac{g_{a\gamma}}{2}\Delta a,$$

(14)

where Δa is the change in a over the photon trajectory. Fluctuations in the axionlike particle field lead to the spatial variation of α. If the axionlike particle is effectively massless during inflation, the primordial power spectrum of the fluctuations of the axionlike particle field is scale invariant. As a result, the cosmic birefringence power spectrum becomes a scale-invariant spectrum in the large-scale limit ($L \lesssim 100$) [25]:

$$\frac{L(L+1)C_L^{\alpha\alpha}}{2\pi} = \left(\frac{H_I g_{a\gamma}}{4\pi}\right)^2.$$

(15)

Here, H_I is the inflationary Hubble parameter and is related to the tensor-to-scalar ratio, r, as $H_I = 2\pi M_{\mathrm{pl}}\sqrt{A_s r/8} \simeq \sqrt{4r} \times 10^{14}$ GeV, where $M_{\mathrm{pl}} \simeq 2 \times 10^{18}$ GeV is the reduced Planck mass and $A_s \simeq 2 \times 10^{-9}$ is the amplitude of the primordial scalar perturbations (see, e.g., Ref. [69]). An axion string network produces a similar scale-invariant spectrum as shown by Ref. [13]. Using Eq. (15), our A_{CB} constraint can be translated into constraints on coupling between axionlike particles and photons as

$$g_{a\gamma} \leq \frac{4.0 \times 10^{-2}}{H_I} = \frac{2.0 \times 10^{-16}}{\sqrt{r}} \text{ GeV}^{-1}$$

(16)

at 10^{-33} eV $\lesssim m_a \lesssim 10^{-28}$ eV. The coupling constant is related to the decay constant, f_a. In string theory models, typically $f_a \sim 10^{16}$ GeV, although it could be the Planck energy scale. Assuming $g_{a\gamma} \sim 10^{-3}/f_a$ [10], the constraint in Eq. (16) can be translated into a constraint on f_a as $10^{-6} \lesssim f_a/H_I$. A detection of the tensor-to-scalar ratio in a future CMB experiment, which would determine H_I, would put a lower bound on f_a from the CMB cosmic birefringence.

The coupling constant of the axionlike particles has been also constrained in various ways and data from astrophysical experiments [70]. The isotropic cosmic birefringence constraint from recent CMB experiments is translated into the constraint on the coupling constant for the axion dark matter as $g_{a\gamma} \lesssim 1.6 \times 10^{-15}(m_a/3 \times 10^{-26}$ eV) GeV^{-1} at $10^{-27} \leq m_a \leq 10^{-24}$ eV [71]. The interaction described in Eq. (13) causes axionlike particles and photons to interconvert in the presence of a background magnetic field, and the axionlike particles could introduce localized oscillatory modulation in the spectra of photon sources passing through astrophysical magnetic fields. By exploring this effect in the recent x-ray spectral data, Refs. [72,73] derive constraints on the coupling constant as $g_{a\gamma} \lesssim 10^{-12}$ GeV^{-1} for $m_a \lesssim 10^{-12}$ eV. Coherent oscillations of the Bose condensate of axionlike particles induce periodic changes in the plane of linear polarization of emission passing

through the condensate. Analysis of polarization observations of bright downstream features in the parsec-scale jets of active galaxies leads to a constraint on the coupling constant as $g_{a\gamma} \lesssim 10^{-12}$ GeV^{-1} for $5 \times 10^{-23} \lesssim m_a \lesssim 10^{-21}$ eV [74]. Compared to the above other constraints on the lower-mass axionlike particles, our constraint on the coupling constant is very stringent if a scenario of large-field inflation models is assumed, $r \gtrsim 0.01$. To directly compare our constraints with other probes, however, the determination of the energy scale of inflation is necessary. This could be achieved by ongoing and future CMB experiments.

Our measured spectrum can also be used to constrain other possible sources of the cosmic birefringence proposed by Refs. [13–15], although constraining these other sources is beyond the scope of this paper.

Measurements of anisotropic cosmic birefringence can be of great importance for testing new physical theories of the early Universe. Future CMB experiments such as the BICEP Array [75], CMB-S4 [76], LiteBIRD [77], Simons Observatory [78], and SPT-3G [79] will measure cosmic birefringence anisotropies even more precisely [80]. In these experiments, a curved-sky polarization analysis, as we have presented here, will be necessary to tightly constrain a scale-invariant spectrum of cosmic birefringence anisotropies, which is one of the physically best-motivated spectra.

ACKNOWLEDGMENTS

APPENDIX A: SEPARABLE FORMS FOR COMPUTING THE COSMIC BIREFRINGENCE QUADRATIC ESTIMATOR

Here we describe computationally efficient ways for calculating the quadratic estimator of cosmic birefringence implemented in https://toshiyan.github.io/clpdoc/html/.

1. Unnormalized quadratic estimator

The unnormalized quadratic estimator is given by

$$\bar{\alpha}_{LM} = \sum_{\ell\ell'mm'} \begin{pmatrix} \ell & \ell' & L \\ m & m' & M \end{pmatrix} (-W^-_{\ell'L\ell}) \tilde{C}^{EE}_\ell \bar{E}_{\ell m} \bar{B}_{\ell'm'}. \qquad (A1)$$

Using the properties of the Wigner $3j$ symbols and the relationship between the Wigner $3j$ symbols and spherical harmonics, we obtain

$$-\begin{pmatrix} \ell & \ell' & L \\ m & m' & M \end{pmatrix} W^-_{\ell'L\ell} = [1 + (-1)^{\ell+\ell'+L}] \sqrt{\frac{(2\ell+1)(2\ell'+1)(2L+1)}{4\pi}} \begin{pmatrix} \ell' & L & \ell \\ -2 & 0 & 2 \end{pmatrix} \begin{pmatrix} \ell & \ell' & L \\ m & m' & M \end{pmatrix}$$

$$= \sqrt{\frac{(2\ell+1)(2\ell'+1)(2L+1)}{4\pi}} \left[\begin{pmatrix} \ell & \ell' & L \\ 2 & -2 & 0 \end{pmatrix} + \begin{pmatrix} \ell & \ell' & L \\ -2 & 2 & 0 \end{pmatrix} \right] \begin{pmatrix} \ell & \ell' & L \\ m & m' & M \end{pmatrix}$$

$$= \int d\hat{n} Y_{LM} [Y^2_{\ell m} Y^{-2}_{\ell'm'} + Y^{-2}_{\ell m} Y^2_{\ell'm'}]. \qquad (A2)$$

Substituting the above equation into Eq. (A1), we obtain the separable form of the quadratic estimator:

$$\bar{\alpha}_{LM} = \int \mathrm{d}\hat{n} Y_{LM}^* \left[\sum_{\ell m} Y_{\ell m}^2 \tilde{C}_\ell^{EE} \bar{E}_{\ell m} \sum_{\ell' m'} Y_{\ell' m'}^{-2} \bar{B}_{\ell' m'} + \sum_{\ell m} Y_{\ell m}^{-2} \tilde{C}_\ell^{EE} \bar{E}_{\ell m} \sum_{\ell' m'} Y_{\ell' m'}^2 \bar{B}_{\ell' m'} \right]$$

$$= \mathrm{i} \int \mathrm{d}\hat{n} Y_{LM}^* [(Q^E + \mathrm{i}U^E)(Q^B - \mathrm{i}U^B) - \text{c.c.}]$$

$$= -2 \int \mathrm{d}\hat{n} Y_{LM}^* [U^E Q^B - Q^E U^B], \tag{A3}$$

where we define the real quantities Q^E, U^E, Q^B, and U^B as

$$Q^E + \mathrm{i}U^E = \sum_{\ell m} Y_{\ell m}^2 \tilde{C}_\ell^{EE} \bar{E}_{\ell m},$$

$$Q^B + \mathrm{i}U^B = \sum_{\ell m} Y_{\ell m}^2 \mathrm{i}\bar{B}_{\ell m}. \tag{A4}$$

2. Normalization

The estimator from the previous section must be normalized [see Eq. (8)]. Here we extend the method for

lensing and delensing used in Ref. [84] to cosmic birefringence. The inverse of the normalization is given by

$$\frac{1}{A_L} = \frac{1}{2L+1} \sum_{\ell \ell'} |W_{\ell' L \ell}^-|^2 a_\ell b_{\ell'}, \tag{A5}$$

where we define $a_\ell = 1/\hat{C}_\ell^{BB}$ and $b_\ell = (\tilde{C}_\ell^{EE})^2/\hat{C}_\ell^{EE}$. Using the relation between the Wigner $3j$ symbols and the Wigner d function, we obtain

$$\frac{1}{A_L} = \pi \sum_{\ell \ell'} \frac{2\ell+1}{4\pi} a_\ell \frac{2\ell'+1}{4\pi} b_{\ell'} 8 \left[\begin{pmatrix} \ell & L & \ell' \\ -2 & 0 & 2 \end{pmatrix}^2 + \begin{pmatrix} \ell & L & \ell' \\ -2 & 0 & 2 \end{pmatrix} \begin{pmatrix} \ell & L & \ell' \\ 2 & 0 & -2 \end{pmatrix} \right]$$

$$= \int_{-1}^1 \mathrm{d}\mu 4\pi \sum_{\ell \ell'} \frac{2\ell+1}{4\pi} a_\ell \frac{2\ell'+1}{4\pi} b_{\ell'} (d_{-2,-2}^\ell d_{00}^L d_{22}^{\ell'} + d_{-2,2}^\ell d_{00}^L d_{2,-2}^{\ell'})$$

$$= \int_{-1}^1 \mathrm{d}\mu 4\pi (\xi_{-2,-2}^a \xi_{22}^b + \xi_{-2,2}^a \xi_{2,-2}^b) d_{00}^L, \tag{A6}$$

where we define

$$\xi_{mm'}^a = \sum_\ell \frac{2\ell+1}{4\pi} a_\ell d_{mm'}^\ell. \tag{A7}$$

APPENDIX B: MEAN-FIELD BIAS IN THE PRESENCE OF A GLOBAL POLARIZATION ANGLE ERROR

Here we describe how the global polarization angle error introduces the mean-field bias in the rotation estimator. Assuming nonzero C_ℓ^{EB}, the off-diagonal elements of the EB correlation induced by lensing have the following additional term containing C_ℓ^{EB}:

$$\langle \bar{E}_{\ell m} \bar{B}_{\ell' m'} \rangle_{\text{CMB}} = \sum_{LM} \begin{pmatrix} \ell & \ell' & L \\ m & m' & M \end{pmatrix} \tilde{f}_{\ell L \ell'}^\phi \phi_{LM}^*, \tag{B1}$$

where $\tilde{f}_{\ell L \ell'}^\phi$ is the usual weight function of the EE quadratic estimator for lensing [41], but replacing the

EE with the EB spectrum. For the finite sky coverage, the window function also produces off-diagonal correlations as

$$\langle \bar{E}_{\ell m} \bar{B}_{\ell' m'} \rangle_{\text{CMB}} = \sum_{LM} \begin{pmatrix} \ell & \ell' & L \\ m & m' & M \end{pmatrix} \tilde{f}_{\ell L \ell'}^\epsilon \epsilon_{LM}^*, \tag{B2}$$

where $\tilde{f}_{\ell L \ell'}^\epsilon$ is the usual weight function of the EE quadratic estimator for the window [59], but replacing the EE with the EB spectrum. The above equations indicate that, if C_ℓ^{EB} is nonzero due to a global polarization error, the lensing and window introduces the following mean-field bias:

$$\langle \hat{\alpha}_{LM} \rangle = \frac{A_L}{2L+1} \sum_{x=\phi,\epsilon} x_{LM} \sum_{\ell \ell'} \frac{f_{\ell L \ell'}^\alpha \tilde{f}_{\ell L \ell'}^x}{\hat{C}_\ell^{EE} \hat{C}_{\ell'}^{BB}}. \tag{B3}$$

We can construct a bias-hardened estimator for $\hat{\alpha}$ in a similar way as Ref. [59]. However, the signal-to-noise ratio of the bias-hardened estimator is significantly degraded.

[1] R. J. Thornton *et al.*, Astrophys. J. Suppl. Ser. **227**, 21 (2016).
[2] T. Louis *et al.*, J. Cosmol. Astropart. Phys. 06 (2017) 031.
[3] B. D. Sherwin *et al.*, Phys. Rev. D **95**, 123529 (2017).
[4] A. van Engelen *et al.*, Astrophys. J. **808**, 9 (2015).
[5] S. M. Carroll, Phys. Rev. Lett. **81**, 3067 (1998).
[6] M. Li and X. Zhang, Phys. Rev. D **78**, 103516 (2008).
[7] M. Pospelov, A. Ritz, and C. Skordis, Phys. Rev. Lett. **103**, 051302 (2009).
[8] F. Finelli and M. Galaverni, Phys. Rev. D **79**, 063002 (2009).
[9] R. Hlozek, D. J. E. Marsh, and D. Grin, Mon. Not. R. Astron. Soc. **476**, 3063 (2018).
[10] D. J. E. Marsh, Phys. Rep. **643**, 1 (2016).
[11] M. A. Fedderke, P. W. Graham, and S. Rajendran, Phys. Rev. D **100**, 015040 (2019).
[12] L. M. Capparelli, R. R. Caldwell, and A. Melchiorri, arXiv: 1909.04621.
[13] P. Agrawal, A. Hook, and J. Huang, arXiv:1912.02823.
[14] G.-C. Liu and K.-W. Ng, Phys. Dark Universe **16**, 22 (2017).
[15] D. Leon, J. Kaufman, B. Keating, and M. Mewes, Mod. Phys. Lett. A **32**, 1730002 (2017).
[16] A. Kosowsky and A. Loeb, Astrophys. J. **469**, 1 (1996).
[17] D. D. Harari, J. D. Hayward, and M. Zaldarriaga, Phys. Rev. D **55**, 1841 (1997).
[18] A. Kosowsky, T. Kahniashvili, G. Lavrelashvili, and B. Ratra, Phys. Rev. D **71**, 043006 (2005).
[19] A. Yadav, L. Pogosian, and T. Vachaspati, Phys. Rev. D **86**, 123009 (2012).
[20] S. De, L. Pogosian, and T. Vachaspati, Phys. Rev. D **88**, 063527 (2013).
[21] L. Pogosian, Mon. Not. R. Astron. Soc. **438**, 2508 (2014).
[22] G. Gubitosi and F. Paci, J. Cosmol. Astropart. Phys. 02 (2013) 020.
[23] A. Lue, L. Wang, and M. Kamionkowski, Phys. Rev. Lett. **83**, 1506 (1999).
[24] C. Li, T. L. Smith, and A. Cooray, Phys. Rev. D **75**, 083501 (2007).
[25] R. R. Caldwell, V. Gluscevic, and M. Kamionkowski, Phys. Rev. D **84**, 043504 (2011).
[26] S. Lee, G.-C. Liu, and K.-W. Ng, Phys. Rev. B **746**, 406 (2015).
[27] V. Gluscevic, M. Kamionkowski, and D. Hanson, Phys. Rev. D **87**, 047303 (2013).
[28] B. Feng, M. Li, J.-Q. Xia, X. Chen, and X. Zhang, Phys. Rev. Lett. **96**, 221302 (2006).
[29] A. Gruppuso, P. Natoli, N. Mandolesi, A. DeRosa, and F. Paci, J. Cosmol. Astropart. Phys. 02 (2012) 023.
[30] S.-Y. Li, J.-Q. Xia, M. Li, H. Li, and X. Zhang, Astrophys. J. **799**, 211 (2015).
[31] H.-H. Mei, W.-T. Ni, W.-P. Pan, L. Xu, and S. di Serego Alighieri, Astrophys. J. **805**, 107 (2015).
[32] L. Pagano, P. de Bernardis, G. de Troia, G. Gubitosi, S. Masi, A. Melchiorri, P. Natoli, F. Piacentini, and G. Polenta, Phys. Rev. D **80**, 043522 (2009).
[33] N. J. Miller, M. Shimon, and B. G. Keating, Phys. Rev. D **79**, 103002 (2009).
[34] B. Keating, M. Shimon, and A. Yadav, Astrophys. J. **762**, L23 (2013).

[35] G. Hinshaw *et al.*, Astrophys. J. **208**, 19 (2013).
[36] N. Aghanim *et al.* (Planck Collaboration), Astron. Astrophys. **596**, A110 (2016).
[37] J. P. Kaufman *et al.*, Phys. Rev. D **89**, 062006 (2014).
[38] P. A. R. Ade *et al.* (BICEP2/Keck Array Collaboration), Phys. Rev. Lett. **121**, 221301 (2018).
[39] Y. Minami, H. Ochi, K. Ichiki, N. Katayama, E. Komatsu, and T. Matsumura, Prog. Theor. Exp. Phys. **2019**, 083E02 (2019).
[40] M. Kamionkowski, Phys. Rev. Lett. **102**, 111302 (2009).
[41] T. Okamoto and W. Hu, Phys. Rev. D **67**, 083002 (2003).
[42] A. P. S. Yadav, M. Shimon, and B. G. Keating, Phys. Rev. D **86**, 083002 (2012).
[43] P. A. R. Ade *et al.* (POLARBEAR Collaboration), Phys. Rev. D **92**, 123509 (2015).
[44] P. A. R. Ade *et al.* (BICEP2/Keck Array Collaboration), Phys. Rev. D **96**, 102003 (2017).
[45] D. Contreras, P. Boubel, and D. Scott, J. Cosmol. Astropart. Phys. 12 (2017) 046.
[46] G. Gubitosi, M. Migliaccio, L. Pagano, G. Amelino-Camelia, A. Melchiorri, P. Natoli, and G. Polenta, J. Cosmol. Astropart. Phys. 11 (2011) 003.
[47] M. Li and B. Yu, J. Cosmol. Astropart. Phys. 06 (2013) 016.
[48] S. di Serego Alighieri, W.-T. Ni, and W.-P. Pan, Astrophys. J. **792**, 35 (2014).
[49] H. Zhai, S.-Y. Li, M. Li, and X. Zhang, Phys. Lett. B **802**, 135240 (2020).
[50] S. Aiola *et al.* (to be published).
[51] S. Choi *et al.* (to be published).
[52] O. Darwish *et al.*, arXiv:2004.01139.
[53] R. Adam *et al.* (Planck Collaboration), Astron. Astrophys. **594**, A9 (2016).
[54] F. Vansyngel, F. Boulanger, T. Ghosh, B. D. Wandelt, J. Aumont, A. Bracco, F. Levrier, P. G. Martin, and L. Montier, Astron. Astrophys. **603**, A62 (2017).
[55] T. Namikawa, Phys. Rev. D **95**, 043523 (2017).
[56] M. Kamionkowski, A. Kosowsky, and A. Stebbins, Phys. Rev. D **55**, 7368 (1997).
[57] M. Zaldarriaga and U. Seljak, Phys. Rev. D **55**, 1830 (1997).
[58] V. Gluscevic, M. Kamionkowski, and A. Cooray, Phys. Rev. D **80**, 023510 (2009).
[59] T. Namikawa, D. Hanson, and R. Takahashi, Mon. Not. R. Astron. Soc. **431**, 609 (2013).
[60] T. Namikawa, D. Yamauchi, and A. Taruya, J. Cosmol. Astropart. Phys. 01 (2012) 007.
[61] N. Aghanim *et al.* (Planck Collaboration), arXiv:1807 .06210 [Astron. Astrophys. (to be published)].
[62] Planck Collaboration, Astron. Astrophys. **571**, A17 (2014).
[63] B. Koopman *et al.*, Proc. SPIE Int. Soc. Opt. Eng. **9914**, 99142T (2016).
[64] R. Adam *et al.* (Planck Collaboration), Astron. Astrophys. **586**, A133 (2016).
[65] Y. Akrami *et al.* (Planck Collaboration), arXiv:1801.04945.
[66] S. Hamimeche and A. Lewis, Phys. Rev. D **77**, 103013 (2008).
[67] S. M. Carroll, G. B. Field, and R. Jackiw, Phys. Rev. D **41**, 1231 (1990).
[68] D. Harari and P. Sikivie, Phys. Rev. B **289**, 67 (1992).
[69] D. Baumann, Inflation, in *Physics of the Large and the Small, TASI 09, Proceedings of the Theoretical Advanced*

Study Institute in Elementary Particle Physics, Boulder, Colorado, USA, 2009 (World Scientific, Singapore, 2011), pp. 523–686.

[70] M. Tanabashi *et al.* (Particle Data Group), Phys. Rev. D **98,** 030001 (2018).

[71] G. Sigl and P. Trivedi, arXiv:1811.07873.

[72] M. Berg, J. P. Conlon, F. Day, N. Jennings, S. Krippendorf, A. J. Powell, and M. Rummel, Astrophys. J. **847,** 101 (2017).

[73] C. S. Reynolds, M. C. D. Marsh, H. R. Russell, A. C. Fabian, R. Smith, F. Tombesi, and S. Veilleux, arXiv:1907 .05475.

[74] M. M. Ivanov, Y. Y. Kovalev, M. L. Lister, A. G. Panin, A. B. Pushkarev, T. Savolainen, and S. V. Troitsky, J. Cosmol. Astropart. Phys. 02 (2019) 059.

[75] H. Hui *et al.*, Proc. SPIE Int. Soc. Opt. Eng. **10708,** 1070807 (2018).

[76] K. Abazajian *et al.* (CMB-S4 Collaboration), arXiv:1907 .04473.

[77] M. Hazumi *et al.*, J. Low Temp. Phys. **194,** 443 (2019).

[78] A. Lee *et al.*, Bull. Am. Astron. Soc. **51,** 147 (2019).

[79] B. A. Benson *et al.*, Proc. SPIE Int. Soc. Opt. Eng. **9153,** 91531P (2014).

[80] L. Pogosian, M. Shimon, M. Mewes, and B. Keating, Phys. Rev. D **100,** 023507 (2019).

[81] A. Zonca, L. Singer, D. Lenz, M. Reinecke, C. Rosset, H. Hivon, and K. Gorski, J. Open Source Software **4,** 1298 (2019).

[82] K. M. Górski, E. Hivon, A. J. Banday, B. D. Wandelt, F. K. Hansen, M. Reinecke, and M. Bartelmann, Astrophys. J. **622,** 759 (2005).

[83] A. Lewis, A. Challinor, and A. Lasenby, Astrophys. J. **538,** 473 (2000).

[84] K. M. Smith, D. Hanson, M. LoVerde, C. M. Hirata, and O. Zahn, J. Cosmol. Astropart. Phys. 06 (2012) 014.